Soft Matter

PAPER

View Article Online
View Journal | View Issue

Published on 19 January 2017. Downloaded by Synchrotron Radiation Library on 20/07/2017 02:15:51.

Cite this: *Soft Matter*, 2017, **13**, 1569

Crystallization behavior of crystalline/crystalline polymer blends under confinement in electrospun nanofibers of polystyrene/poly(ethylene oxide)/poly(ε-caprolactone) ternary mixtures†

Pratick Samanta,[a] Rajiv Srivastava,[a] Bhanu Nandan*[a] and Hsin-Lung Chen*[b]

Received 9th December 2016,
Accepted 18th January 2017

DOI: 10.1039/c6sm02748b

rsc.li/soft-matter-journal

We have studied the crystallization behavior of crystalline/crystalline blends of poly(ethylene oxide) (PEO) and poly(ε-caprolactone) (PCL) in electrospun nanofibers fabricated from ternary blends of polystyrene (PS), PEO, and PCL, where PS was present as the majority component. It was demonstrated previously that PEO in PS/PEO binary blend nanofibers with a low PEO weight fraction (≦0.2) crystallized predominantly through homogenous nucleation due to the small PEO domain size which excluded the presence of heterogeneities (*Soft Matter*, 2016, **12**, 5110). Here, it was found that PCL in PS/PCL binary blend nanofibers exhibited similar behavior, but at a much lower weight fraction of PCL (≦0.1) due to the presence of an inherently higher concentration of heterogeneities in the PCL homopolymer. In the PS/PEO/PCL ternary blend nanofibers, where the combined weight fraction of PEO and PCL was kept at 0.2 or less, the crystallization of the two components took place separately through both heterogeneous and homogenous nucleation mechanisms. The phase segregated crystallization behavior was further confirmed by the melting behavior of the blend nanofibers and wide angle X-ray diffraction (WAXD) measurements. Most significantly, the homogenous nucleation of both PEO and PCL was suppressed whereas the heterogeneous nucleation was enhanced in the ternary blend nanofibers even at very low weight fraction of PEO or PCL. This was plausibly attributed to the coupling between the crystallization and the liquid–liquid phase separation (LLPS) of the PEO/PCL mixture dispersed in the PS matrix during non-isothermal cooling of the blend nanofibers. Furthermore, it was observed that thermal treatment of the PS/PEO/PCL blend nanofibers above the glass transition temperature of PS further promoted the heterogeneous nucleation-initiated crystallization of PEO because of a complex interplay between Plateau–Rayleigh instability-induced domain breakup and its further coalescence and demixing within the PEO/PCL domains embedded in the PS matrix.

Introduction

The crystallization behavior of polymer blends has been extensively studied in the past in order to design novel polymer materials with desired properties.[1–3] Most of these studies have been conducted on binary blend systems consisting of an amorphous and a semicrystalline polymer. In this case, the crystallization behavior of the crystallizable polymer depends to a large extent on the miscibility of the two polymers in the melt state. For immiscible polymer blends, a liquid–liquid phase separation occurs prior to the crystallization, such that the crystallization behavior remains nearly identical to that of the neat homopolymer. However, in miscible polymer blends, a liquid–solid phase separation between the two components driven by the crystallization takes pace. In such systems, it has been found that the amorphous component is excluded from the crystallites, which in turn retards the crystallization kinetics and results in the formation of a diverse range of morphological patterns characterized by the location of the amorphous component that is segregated by the crystallization.[4–9]

The crystallization and phase behavior become much more complex when both the constituting polymers of the blend have the ability to crystallize.[10–19] The difference in the melting temperature of the two polymers influences their crystallization

[a] *Department of Textile Technology, Indian Institute of Technology Delhi, Hauz Khas, New Delhi 110016, India. E-mail: nandan@textile.iitd.ac.in*
[b] *Department of Chemical Engineering and Frontier Centre of Fundamental and Applied Sciences of Matters, National Tsing-Hua University, Hsinchu 30013, Taiwan. E-mail: hlchen@che.nthu.edu.tw*

† Electronic supplementary information (ESI) available: Heat of fusion of PS/PCL nanofibers and cast films at various compositions; DSC cooling and heating plots of PEO/PCL films at different compositions; the melting curve of PS/PEO/PCL nanofibers after cooling to a pre-decided temperature from 90 °C; the SEM micrograph of N-S90E05L05 nanofibers; the SAXS pattern of PS/PEO/PCL nanofibers and cast films after isothermal crystallization at −20 °C; and the WAXD pattern of N-S80E10L10 nanofibers crystallized at different temperatures. See DOI: 10.1039/c6sm02748b

Published on 19 January 2017. Downloaded by Synchrotron Radiation Library on 20/07/2017 02:15:51.

sequence and hence the morphology of the blends. If the two components are miscible in the melt, the polymer with the higher melting point may crystallize first upon cooling which excludes the lower-melting polymer. As a consequence, the crystallization of the lower-melting component may occur in the confined environment, such as the interlamellar regions or the regions between the lamellar bundles, established by the crystallization of the higher-melting polymer. In case where the components have similar melting points, simultaneous crystallization may occur leading to the formation of interpenetrating spherulites. Another factor which influences the crystallization and morphology is the extent of miscibility between the two crystallizable polymers in the melt state. The phase separation could be driven by the intrinsic repulsive interaction between the two polymers (dictated by the Flory–Huggins interaction parameter) or by a combination of the repulsive interaction and crystallization-induced liquid–solid phase separation. The cocrystallization of the two components into one crystalline phase in the crystalline/crystalline blend is rare due to the strict selection rule in crystallographic packing and conformation.

Recently, crystallization of polymers in a confined space has received significant attention.[20–28] The nano-confinement may frustrate the crystal growth and in turn results in an obvious deviation of the crystallization behaviour from that known for the bulk conditions. Under nano-confined conditions, the number of domains per unit volume is much higher than the number density of heterogeneities present; hence, a predominant fraction of the polymer chains in the confined space has to crystallize through a self-nucleation or homogeneous nucleation mechanism which takes place at very large degrees of supercooling. In the past, the confined crystallization behaviour of polymers has been studied mostly using microphase-separated nanodomains of block copolymers, nanoporous anodic alumina (AAO) membranes and multilayer thin films for constructing the confined environment.[29–44] A number of interesting phenomena have been reported utilizing these systems. One of them is the dominance of the homogeneous nucleation mechanism when the confined length scale is sufficiently small, generally less than 100 nm.[45–47] It has also been observed that nucleation may even become completely suppressed if the confinement, in at least one direction, is below about 20 nm.[47] Under such strong confinement the surface energy of the crystals plausibly prevails over their bulk lattice energy. Apart from the difference in the nucleation mechanism, it has also been found that the crystallization rate, degree of crystallinity and melting point decrease when the crystallization occurs in a confined space.[30,48–51] Spatial confinement also induces the crystallites to adopt a preferred orientation in the confined space,[23] and may alter the polymorphism behaviour of the crystallites.[52,53]

Most studies on confined crystallization have been performed on homopolymers. The crystallization behavior under confinement for a crystalline/crystalline polymer blend is expected to be much more complex. However, until now, investigation in this direction is still limited. More significant work has been reported using a mixture of crystalline–amorphous diblock copolymers where the amorphous block forms the matrix and the two different crystalline blocks are mixed intimately in the self-assembled microdomains in the melt state. Chen and coworkers demonstrated that the crystallization behavior of poly(L-lactic acid) (PLLA) was significantly affected when it was confined, together with poly(ethylene oxide) (PEO), within the lamellar domains of blends of polystyrene-*block*-poly(ethylene oxide) (PS-*b*-PEO) and PS-*b*-PLLA.[54] In another study, they demonstrated that the PEO of two different molecular weights co-crystallized within the lamellar microdomains formed by a mixture of two polybutadiene-*block*-poly(ethylene oxide) (PB-*b*-PEO) with different molecular weights.[55] This was contrary to the phase-segregated crystallization observed for the corresponding mixture of PEO homopolymers.[56–59] Similarly, it was observed that in polystyrene-*block*-poly(ethylene oxide)-*block*-poly(ε-caprolactone) (PS-*b*-PEO-*b*-PCL), PEO and PCL could crystallize and melt coincidentally depending on the composition of the triblock copolymer as well as the crystallization temperature.[60] Recently, Floudas and coworkers have studied the crystallization behavior of PEO-*b*-PCL double crystalline diblock copolymers confined in nanoporous AAO membranes.[61] It was observed that nucleation of PEO was completely suppressed due to double confinement imposed by the AAO rigid wall and the PCL crystals which had a higher melting point than the PEO.

All the previous studies on confined crystallization of crystalline/crystalline polymer blends involved block copolymers where the significant deviation from the bulk crystallization behavior observed may be due to the confinement effect coupled with the restriction imposed by the junction point either between the amorphous and the crystalline blocks or between the two crystalline blocks. In the present study, we study the confined crystallization behavior of the blends involving two crystalline homopolymers *i.e.* PEO and PCL, without using their block copolymers as the template. The confined environment was constructed using electrospun nanofibers of the blends of PS, PEO and PCL, where PS was present in majority such that PEO and PCL formed the dispersed phase embedded in the PS matrix in the nanofibers. In the electrospun nanofibers of this type of blend, the limited radial dimension of the nanofibers may restrict the length scale of phase separation between the immiscible constituents, so as to generate the domains in nanodimensions. Since the melting points of both PEO and PCL are well below the glass transition temperature of PS, the crystallization and melting of the PEO/PCL phase were expected to occur within the confined space surrounded by the glassy PS matrix. We will demonstrate that the PEO/PCL blend under confinement exhibited fractioned crystallization behavior where PEO and PCL exhibited both heterogeneous and homogenous nucleation and the two constituents underwent phase segregated crystallization. Most significantly, the homogenous nucleation of PEO and PCL was suppressed whereas the heterogeneous nucleation was found to be enhanced in the ternary blend nanofibers even at very low weight fractions of PEO or PCL, contrary to the dominance of homogenous nucleation expected under such conditions. It will be shown that the promotion of heterogeneous nucleation was due to the coupling between the crystallization and the concentration fluctuations of liquid–liquid phase separation of the PEO/PCL mixture dispersed in the PS matrix in the ternary blend nanofibers. Furthermore, the confinement led to a significant

 This journal is © The Royal Society of Chemistry 2017

Published on 19 January 2017. Downloaded by Synchrotron Radiation Library on 20/07/2017 02:15:51.

decrease in the melting points of both polymers compared to those in the bulk. The present study provides new insights into the effect of confinement on the crystallization behavior in crystalline/crystalline blends in the absence of junction point constraint.

Results and discussion

The crystallization behaviour of PCL and PEO homopolymers dispersed in the PS matrix in the nanofibers will be first discussed before presenting the crystallization behaviour of the PCL/PEO blends. The crystallization of PEO confined in the electrospun nanofibers of PS/PEO blends has already been reported previously.[62] The PS/PEO blends are known to be immiscible, and the temperature dependence of the Flory–Huggins interaction parameters (χ) between PEO and PS is given by the following equation:[62]

$$\chi_{PS/PEO} = -0.000705 + 21.3/T \quad (1)$$

where T is the temperature in Kelvin. The equation shows that $\chi_{PS/PEO}$ remains positive over a wide range of temperatures. Hence, PS and PEO were expected to be immiscible in the melt state, where these two polymers are always phase-separated into two phases with essentially pure composition. The electrospun nanofibers of PS/PEO blends were found to display significantly different crystallization behaviour from those in the bulk, which depended on the blend composition as well as the melt annealing temperature. The nanofibers with low PEO weight fraction ($\leqq$0.2) crystallized predominantly through homogenous nucleation because the small PEO domain size excluded the presence of heterogeneities. An abrupt transformation in the crystallization nucleation mechanism was observed when the weight fraction of PEO in the blend nanofibers was increased from 0.2 to 0.3, where the heterogeneous nucleation became dominant due to the presence of a larger PEO domain size with spatial connectivity. However, when the blend nanofibers with a PEO weight fraction of 0.3 were crystallized after melt annealing at temperatures greater than the T_g of the PS matrix, the homogenous nucleation mechanism was also observed along with the heterogeneous mechanism. This was attributed to the reduction of PEO domain size due to Plateau–Rayleigh instability-induced domain breakup during melt annealing of the nanofibers. At further higher melt annealing temperatures, the coalescence of the PEO domains became the dominating factor which increased the domain size, such that the crystallization occurred preferably through the heterogeneous nucleation mechanism. The crystallization behaviour of the PCL homopolymer in electrospun nanofibers of PS/PCL blends was investigated in the present study and will be discussed in the following section.

PS/PCL binary blends

Table 1 summarizes the optimized conditions to obtain uniform and bead-free nanofibers of PS/PCL blends.

Electrospun nanofibers. Fig. 1 shows the SEM micrographs of the electrospun nanofibers of PS/PCL blends with different compositions. The electrospinning conditions were optimized to obtain bead-free uniform fibers. The electrospinning was conducted using a 70/30 mixture of DMF/DCM as the solvent. PCL does not readily dissolve in DMF and hence DCM was used to increase its solubility. The solution viscosity is one of the major factors which influences the electrospinning process to achieve uniform smooth fibres.[63–66] Accordingly, the solution concentration for the electrospinning of the PS/PCL blends depended on the composition of the constituting polymers. A higher solution concentration was needed for the blends with a higher PCL content due to the low molecular weight of the PCL ($M_w \sim 60\,000$ g mol^{-1}) used compared to that of PS ($M_w \sim 190\,000$ g mol^{-1}). Fig. 1 reveals that smooth and mostly bead-free nanofibers were produced under the optimized conditions. The average diameter of the nanofibers was found to be 1.57, 1.00 and 1.31 μm for N-S90L10, N-S80L20 and N-S70L30, respectively. Hence, the fiber diameters were nearly the same in all cases.

Crystallization behavior. The crystallization behaviour of PCL in PS/PCL blend nanofibers and bulk films was investigated using a combination of DSC and WAXS. The temperature dependence of the Flory–Huggins segmental interaction parameters (χ) between PCL and PS is given by the following equation:[67]

$$\chi_{PS/PCL} = -0.0143 + 18.186/T \quad (2)$$

where T is the temperature in Kelvin. The equation shows that $\chi_{PS/PCL}$ remains positive over the temperature range studied. Hence, PS and PCL were expected to be immiscible in the melt state, and the crystallization of PCL occurred predominantly within the PCL-rich domains. It is noted that the $\chi_{PS/PEO}$ is indeed more positive[62] than $\chi_{PS/PCL}$, such that the degree of miscibility of the PS/PEO blend was poorer than PS/PCL. Fig. 2 shows the DSC curves collected in the cooling and subsequent heating cycles for recording the crystallization exotherms and melting endotherms, respectively, of PCL in the cast films and the nanofibers. The neat PCL film was found to crystallize with a peak crystallization temperature (T_c) of *ca.* 34 °C upon cooling

Table 1 Electrospinning parameters for different PS and PCL compositions and respective sample codes

Sl. no.	Sample name (nanofibers)	Sample code	Process parameters			
			Conc. (wt%)	Distance (cm)	Voltage (kV)	Flow rate (ml h^{-1})
1	PS-70%, PCL-30%	S70L30	14	20	20	0.5
2	PS-80%, PCL-20%	S80L20	11	20	20	0.5
3	PS-90%, PCL-10%	S90L10	10	20	20	0.5

The bulk and nanofiber blend samples were differentiated by adding the prefixes C and N, respectively, to the blend composition codes.

Published on 19 January 2017. Downloaded by Synchrotron Radiation Library on 20/07/2017 02:15:51.

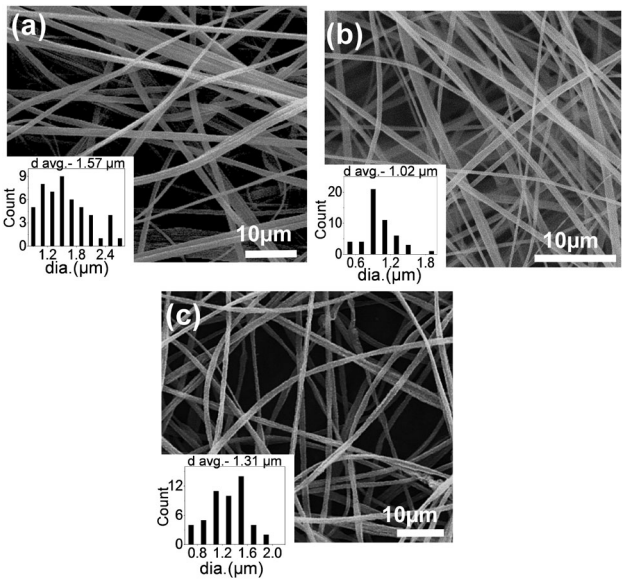

Fig. 1 SEM micrographs of electrospun PS/PCL blend nanofibers: (a) N-S90L10; (b) N-S80L20; (c) N-S70L30. The inset in each figure shows the corresponding distribution of nanofibers diameters.

from melt (see Fig. 2(a)). The crystallization at such a low supercooling temperature is known to occur *via* a heterogeneous nucleation mechanism which is prevalent for crystallization in the bulk state. The PS/PCL blend films displayed almost the same T_c as that of neat PCL irrespective of composition (see Fig. 2(a)), showing that the PCL-rich domains in the phase-separated blends were virtually pure in composition. Moreover, the dominance of the heterogeneous nucleation mechanism implies that the average size of these domains was sufficiently large, such that the number density of the PCL-rich domains was still less than that of the heterogeneous nuclei present.

As shown in Fig. 2(c), the crystallization of neat PCL nanofibers occurred at almost the same supercooling temperature as that of the corresponding film, indicating that the volume of the individual fiber was not small enough to result in homogeneous crystallization. The crystallization behaviour of PCL in the blend nanofibers, however, was found to be composition dependent. The T_c's of the nanofibers containing 20 wt% or more PCL content were only within 8 °C difference from that of neat PCL nanofibers or the film, signaling that the crystallization in the PCL-rich domains developed in the nanofibers proceeded through the heterogeneous nucleation mechanism. However, when the PCL content was decreased to 10 wt% (*i.e.*, for the N-S90L10 blend nanofiber), the cooling curve showed multiple crystallization peaks, as can be seen in the enlarged DSC profile displayed in the inset of Fig. 2(c). The first two peaks centered at ~26 °C and 11 °C were very faint, whereas the third peak observed at much higher supercooling temperature (T_c ~ −14 °C) was relatively more dominant. The DSC cooling experiment thus revealed that the crystallization mechanism in the blend nanofibers with a low PCL composition ($w_{PEO} \leqq 0.1$) differed not only from that of the PS/PCL blend nanofibers with a higher PCL content but also from that of the films with similar compositions.

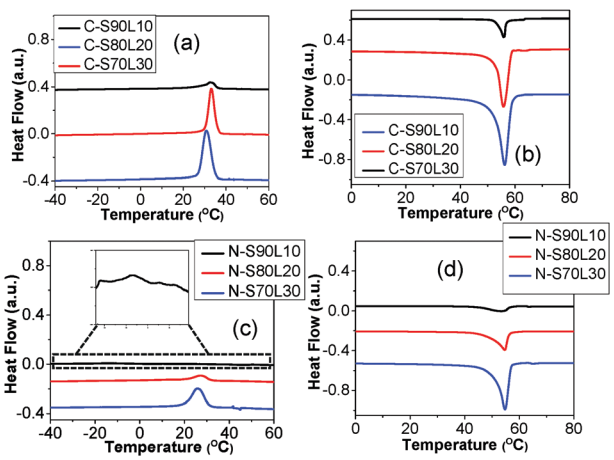

Fig. 2 DSC cooling (a and c) and heating (b and d) curves of PS/PCL blends after first heating up to 90 °C: (a and b) cast film samples and (c and d) nanofiber samples. The inset shows enlarge view of exothermic peaks of N-S90E10 sample.

The crystallization observed at high supercooling temperatures for the blend nanofibers with a low PCL composition can be explained by the dominance of homogeneous nucleation arising from the effect of fractionated crystallization. It is known that a crystalline polymer generally crystallizes *via* the heterogeneous nucleation mechanism where the inherent heterogeneities/impurities present in the polymer act as the nucleating agents. However, if a given volume of the polymer is partitioned into smaller domains such that the number density of such well-separated domains is much larger than that of the heterogeneities present, the polymer in a great fraction of the domains can only crystallize *via* homogenous nucleation, which generally occurs at much higher supercooling temperatures. Chen and co-workers showed that the PEO block in microphase-separated polybutadiene-*block*-poly(ethylene oxide) (PB-*b*-PEO) block copolymers crystallized predominantly through the homogenous nucleation mechanism when it formed cylindrical or spherical nanodomains embedded in the PB matrix.[68–70] Similarly, when the PEO or PCL homopolymer was infiltrated in nanopores of an AAO membrane with pore diameters ranging from 200 to 25 nm, the crystallization was observed to occur predominantly through the homogenous nucleation mechanism as the pore diameter was lowered.[45] It was noted that when the pore size was small, the heterogeneities were retained only in a few pores whereas the large pore size made it possible for most of the pores to contain heterogeneities considering the same volume of polymers in both cases. The T_c corresponding to the homogenous nucleation mechanism was found to decrease with decreasing pore diameter plausibly because of the restriction imposed on chain diffusion/mobility in smaller pores.

In the present study, considering that the PCL in the PS/PCL blends under study was the minor component, PCL was expected to form the dispersed phase in the PS matrix. In the cast films, the size of the PCL dispersed domains was typically a few micrometers, such that heterogeneous nucleation became the dominant nucleation mechanism. However, the small diameter of the nanofibers inhibited the coarsening of the PCL domains, thereby restricting

 This journal is © The Royal Society of Chemistry 2017

Published on 19 January 2017. Downloaded by Synchrotron Radiation Library on 20/07/2017 02:15:51.

the PCL domain size to a few tens or hundreds of nanometers. This led to a situation where the number of PCL domains per unit volume became much higher than that of the heterogeneities present so as to suppress the heterogeneous nucleation process. Hence, the dominant crystallization exotherm observed at $T_c \sim -14$ °C was due to the homogenously nucleated crystallization of PCL in N-S9L1 nanofiber blends. Floudas *et al.* also observed homogenous nucleation at a similar degree of supercooling for PCL confined in nanoporous AAO membranes when the pore size was *ca.* 65 nm. This also suggested that in the N-S90L10 nanofiber blends, the diameter of most of the PCL fibril domains was as small as 65 nm. Furthermore, apart from the small crystallization exotherm observed at $T_c \sim 26$ °C due to heterogeneous nucleation and the dominant exotherm at $T_c \sim -14$ °C due to homogenously nucleated crystallization, a small crystallization exotherm was also observed at $T_c \sim 11$ °C. A similar observation was also made by Floudas and co-workers for PCL infiltrated in an AAO membrane and they attributed it to surface nucleation from the AAO wall.[46] Hence, in the present system, it is plausible that the crystallization exotherm observed at $T_c \sim 11$ °C was due to surface nucleation from the confining glassy PS surface.

The crystallization behaviour observed for PCL in PS/PCL nanofiber blends was similar to that of PEO in PS/PEO blends reported in our earlier study. However, in the case of PS/PEO blends the transition from the heterogeneous to the homogenous nucleation mechanism was observed when the weight fraction of PEO decreased from 0.3 to 0.2. Whereas for PCL this transition was observed at a lower PCL weight fraction of 0.1. This is due to the fact that different polymers may show different crystallization behaviour even when they are confined in a similar geometrical space. It was shown that while isotactic polypropylene (iPP) and poly(ε-caprolactone) (PCL) required much smaller size of confinement to crystallize *via* homogenous nucleation, such a nucleation mechanism was accessible for PEO at a comparatively large geometrical confinement size,[46,47] due to an inherently higher number of heterogeneities present in iPP and PCL compared to that in PEO. Hence, the volume per nucleus in iPP and PCL was much smaller which required a smaller confinement volume to exclude the nuclei so that homogenous nucleation could be accessed.

Furthermore, as shown in Fig. 2(b), the melting points of the PCL in the PS/PCL blend cast films were found to be almost the same as that of the neat PCL homopolymer. However, in the case of PS/PCL nanofibers, the PCL melting point gradually decreased with the decrease of PCL composition in the blend. In the case of N-S90L10, the T_m of PCL was depressed by as much as 4 °C compared to that of neat PCL nanofibers. The reduction of melting point suggested that the lamellar thickness of PCL crystallites developed in the nanofibers, particularly at lower weight fractions, was significantly thinner than that in bulk PCL. The depression in the melting point is explained well by the classical Thomson–Gibbs equation considering a rectangular shaped crystal.[71]

$$T_m = T_m^\circ \left[1 - \left(\frac{\sigma_1}{L_1} + \frac{\sigma_2}{L_2} + \frac{\sigma_3}{L_3}\right)\frac{2}{\rho_c \Delta H_m^\circ}\right] \quad (3)$$

Here, σ_1, σ_2, and σ_3 denote the specific surface free energies of the crystallite; L_1, L_2, and L_3 are the dimensions of the crystallite where the subscripts denote the three orthogonal directions in a chain-folded lamellae; T_m is the observed melting temperature; T_m° and ΔH_m° are the equilibrium melting temperature and heat of fusion per unit mass of crystal with infinite thickness, respectively, and ρ_c is the crystal density. This equation shows that T_m decreases as the crystallite dimension decreases in either direction. In the bulk, the lateral dimensions of the crystallite are much larger than the thickness (*i.e.* $L_2 \gg L_1$ and $L_3 \gg L_1$), such that the terms in the equation containing L_2 and L_3 are neglected. In this case, L_1 and σ_1 representing the crystal thickness and fold surface free energy, respectively, dictate the melting point depression. Under confined conditions, the *c*-axis, *i.e.* the thickness direction of the crystalline lamellae, normally aligns perpendicularly to the long axis of the confining geometry since this orientation provides maximum opportunity for the kinetic growth of the crystallites. Furthermore, the finite dimension of the confined geometry restricts the growth of crystallites in the lateral dimensions. Considering that the PCL domains were fibrillar in shape (to be demonstrated later in Fig. 9), the crystal growth in the lateral direction normal to the long axis of the fibrillar domains was restricted by the fibril diameter.[62] Moreover, once the overall crystallization is dominated by the nucleation, the crystal growth along the long axis of the fibril will also be restricted because of multiple nucleation events in the same domain. Hence, in such confined domains, the lateral surface areas of the crystals become important and the corresponding surface free energies, σ_1 and σ_2 significantly contribute to the overall depression of T_m.

The heat of fusion per unit weight of PCL, which is a measure of the degree of crystallinity, of PCL, for bulk films was less than that of neat PCL. This demonstrated that, even in bulk samples, the crystallization of PCL was influenced in the presence of PS. However, the crystallinity in the nanofibers was much lower and was found to be lowest when the PCL composition was reduced to 10 wt% (please see ESI†). As has already been indicated, the PCL domains were expected to be small and well partitioned in the PS matrix at lower PCL weight fractions; hence, the suppression of crystallizability could be attributed to the restricted growth of the crystallites in the geometrically mismatched and nanoscopically confined PCL domains. It is also noted that the drop of ΔH_m in the blend nanofibers occurred coincidently with the change of the nucleation mechanism from heterogeneous to predominately homogenous type. Such reductions in the heat of fusion and crystallinity were also observed by Floudas and coworkers in the case of PEO and PCL confined in a nanoporous AAO membrane.[45,46] Similarly, Shin *et al.* observed a drastic reduction in the degree of crystallinity of linear polyethylene (PE) confined in an AAO membrane.[71]

PS/PEO/PCL ternary blends

Since most of the anomalous behavior of PEO and PCL crystallization in the electrospun nanofibers was observed when the weight fraction of the crystallizable polymers dispersed in the PS matrix was less than 0.2, studies on the PS/PEO/PCL ternary blends were mostly conducted for the blend compositions

Published on 19 January 2017. Downloaded by Synchrotron Radiation Library on 20/07/2017 02:15:51.

Table 2 Electrospinning parameters for different PS, PEO and PCL compositions and respective sample codes

Sl. no.	Sample name (nanofibers)	Sample code	Process parameters			
			Conc. (wt%)	Distance (cm)	Voltage (kV)	Flow rate (ml h^{-1})
1	PS-80%, PEO-20%, PCL-0%	S80E20L0	8	20	20	0.5
2	PS-80%, PEO-15%, PCL-05%	S80E15L05	8	20	20	0.5
3	PS-80%, PEO-10%, PCL-10%	S80E10L10	8	20	20	0.5
4	PS-80%, PEO-05%, PCL-15%	S80E05L15	8	20	20	0.5
5	PS-80%, PEO-0%, PCL-20%	S80E0L20	10	20	20	0.5
6	PS-70%, PEO-15%, PCL-15%	S70E15L15	6	20	20	0.5
7	PS-90%, PEO-05%, PCL-05%	S90E05L05	10	20	20	0.5

The bulk and nanofiber blend samples were differentiated by adding the prefixes C and N, respectively, to the blend composition codes.

where the combined weight fraction of PEO and PCL ($w_{PEO/PCL}$) in the ternary blends was maintained at 0.2.

Electrospun fibers. Table 2 summarizes the optimized conditions to obtain uniform and bead-free nanofibers of PS/PEO/PCL blends where the total weight fraction of PEO/PCL was kept at 0.2. The surface morphology of the electrospun nanofibers of PS/PEO/PCL with different blend compositions observed under a SEM is shown in Fig. 3. The micrographs show that uniform and bead-free nanofibers were produced under the optimized electrospinning conditions. The distribution of the nanofiber diameter is shown as insets in each of the SEM micrographs. The average diameter of the nanofibers was maintained at 1.5 ± 0.4 μm. Additionally, PS/PEO/PCL electrospun nanofibers were prepared from 90/05/05 compositions. The average nanofiber diameter was found to be 1.45 μm for this blend composition (please see ESI†).

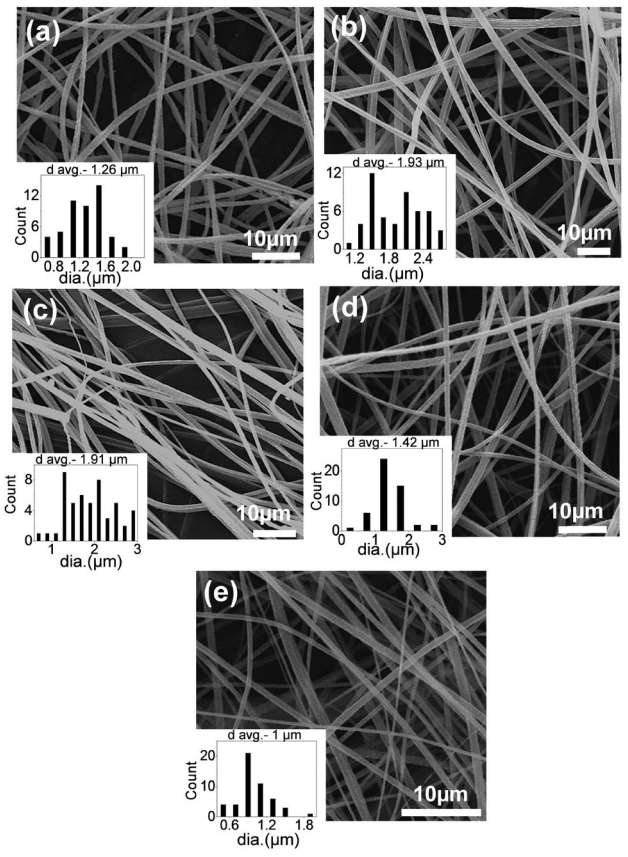

Fig. 3 SEM micrographs of electrospun PS/PEO/PCL blend nanofibers: (a) N-S80E20L00; (b) N-S80E15L05; (c) N-S80E10L10; (d) N-S80E05L15; (e) N-S80E00L20. The inset in each figure shows the corresponding distribution of nanofibers diameters.

The nanofiber diameter depended on a complex interplay among different parameters such as the molecular weights of the polymers, critical entanglement molecular weight, and the solution concentration. It must be noted that we did not observe any significant effect of polydispersity in the diameter of electrospun fibers on the crystallization behavior of PEO/PCL *vis-à-vis* compositional variations in the blends since most of the significant observations were a direct result of the change in the polymer concentrations.

Crystallization behavior. The crystallization behavior of PEO and PCL in the ternary blend was investigated using DSC and WAXS. Earlier studies on the miscibility of PEO/PCL binary blends have revealed a miscibility window of upper critical solution temperature (UCST) character. These blends are miscible well above the melting temperature ($T > 130$ °C) and show liquid–liquid phase separation below the UCST.[72–74] Hence, the crystallization of PEO and PCL occurs within the already macrophase-separated domains in the blend. The crystallization behavior of PEO and PCL was hence expected to remain largely unaffected in the PEO/PCL blends. Here, for comparison, a crystallization study was performed on PEO/PCL binary blends for the same compositions as was present in the PS/PEO/PCL blends. The DSC results showed that the crystallization and the melting peak temperature obtained during cooling and the subsequent heating cycle for PEO and PCL in the binary blends was almost the same as that for respective neat homopolymers (see ESI†). A slight decrease in both the crystallization peak and melting temperatures of PEO and PCL in the blends was observed and was attributed to the presence of a small fraction of PCL and PEO in the PEO-rich and PCL-rich domains, respectively.

Next, DSC studies were performed on PS/PEO/PCL ternary blends in the form of cast films and electrospun nanofibers to reveal the crystallization behavior of PEO and PCL. Fig. 4 shows the DSC curves collected in the cooling and subsequent heating cycles for recording the crystallization exotherms and melting endotherms, respectively, of PEO and PCL. The DSC cooling and heating curves of the PS/PEO/PCL cast films (Fig. 4(a) and (b)) were similar to those observed for the PEO/PCL binary blends, which displayed crystallization and melting behavior

 This journal is © The Royal Society of Chemistry 2017

Published on 19 January 2017. Downloaded by Synchrotron Radiation Library on 20/07/2017 02:15:51.

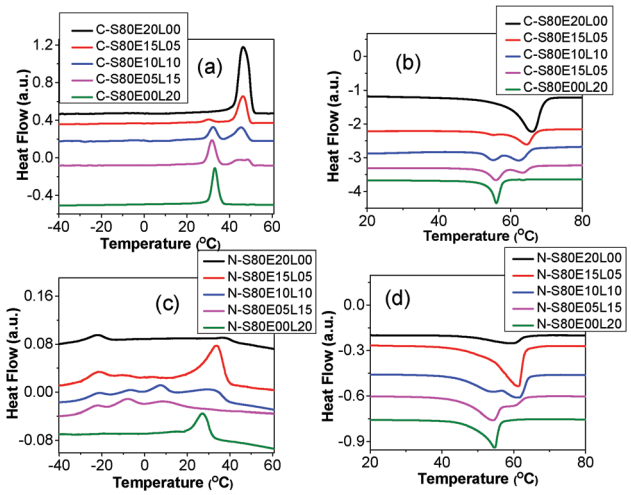

Fig. 4 DSC cooling (a and c) and heating (b and d) curves of PS/PEO/PCL blends after first heating up to 90 °C: (a and b) cast film samples and (c and d) nanofiber samples.

typical of the neat polymers. However, the depression in the melting temperature of PEO with increasing PCL concentration was more obvious in the ternary blends. This could be explained as follows.

In the three-component system, the ultimate morphology of the blend is governed by the mutual solubility of the three components which could be quantified by the Flory–Huggins interaction parameter (χ) or their respective solubility parameters (δ). Since the experimental $\chi_{PCL/PEO}$ was not available in the literature, the solubility parameters of the homopolymers were used to assess their relative solubility. The solubility parameter of PS (δ_{PS}), PEO (δ_{PEO}) and PCL (δ_{PCL}) was found to be 18.6, 20.2, and 19.7 $MPa^{1/2}$, respectively.[75] This indicates that PEO/PCL mixtures were more compatible than PS/PEO and PS/PCL. Furthermore, the compatibility of PS/PCL was also expected to be better than that of PS/PEO. Hence, while the phase separation occurred in the PS/PEO/PCL ternary mixture, the energetically favorable morphology was likely to consist of the phase-separated domains formed by the PEO/PCL mixture dispersed in the PS matrix. This was clearly revealed from the SEM characterization of the fractured samples of the ternary blend. Fig. 5 shows the SEM micrograph of a cryogenically fractured surface of cast film ternary blend samples. The fractured samples were treated with deionized water to remove the PEO phase. The micrograph shows the presence of craters or droplets embedded in the PS matrix.

Craters were observed in the C-S80E15L05 blend whereas droplets were observed in the C-S80E10L10 and C-S80E05L15 blends. The micrographs further show the presence of holes in the droplets embedded in the PS matrix. This could be explained as follows. During the solvent evaporation in film casting, PCL and PEO first phase separated from PS to form dispersed domains composed of a PEO/PCL mixture; further phase separation of PEO and PCL occurred subsequently within these domains. Hence, in the C-S80E15L05 blend where the PCL was expected to be dispersed in the PEO droplet phase, etching with water led to the removal of a complete PEO/PCL

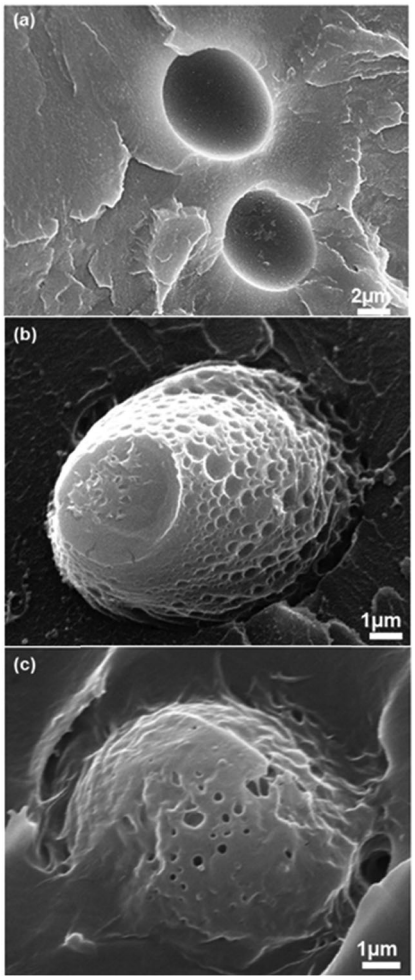

Fig. 5 SEM micrographs of the cross-section of the cast films composed of PS/PEO/PCL blends: (a) C-S80E15L05; (b) C-S80E10L10; (c) C-S80E05L15. The PEO phase was selectively etched using deionized water.

domain leaving craters in the PS matrix. However, in the C-S80E10L10 and C-S80E05L15 blends, the dispersed phase constituted a continuous PCL phase with embedded PEO droplets. The etching with water in this case only led to the removal of PEO droplets embedded in the continuous PCL phase constituting the PEO/PCL droplets. The SEM micrographs in this case, hence, showed the presence of holes in the PCL droplet embedded in the PS matrix. Hence, the SEM results clearly revealed the presence of a combined PEO/PCL droplet phase dispersed in the PS matrix.

Now, the mobility of PEO and PCL was likely to be restricted because of their confinement within the dispersed microdomains. The restricted chain mobility disturbed the phase separation process and, hence, PCL chains plausibly were kinetically trapped within the lamellar structure formed during the PEO crystallization. This led to the formation of more defective PEO crystals and, hence, resulted in a lower melting point.

The DSC cooling and re-heating curves of PS/PEO/PCL electrospun nanofibers are shown in Fig. 4(c) and (d). The crystallization behavior of the nanofibers from the ternary blend was found to be distinctly different from that of the cast films. The ternary blend nanofibers showed multiple crystallization peaks originating from

Published on 19 January 2017. Downloaded by Synchrotron Radiation Library on 20/07/2017 02:15:51.

fractionated crystallization behavior of PEO and PCL confined in the PS glassy matrix. The ternary blend nanofibers displayed four prominent crystallization exotherms located between 25–35 °C, 0–10 °C, −10 to 0 °C, and −25 to −20 °C. To resolve the origin of the crystallization exotherms, the melting endotherms after cooling the sample to the prominent crystallization peaks were recorded. It was found that the crystallization exotherm observed between 25 and 35 °C was exclusively due to the surface/heterogeneous nucleated crystallization of the PEO homopolymer (please see ESI†). The crystallization exotherm between 0 and 10 °C was likely due to the surface/heterogeneous nucleation of PCL whereas that between −10 to 0 °C and −25 to −20 °C was due to homogenous nucleated crystallization of PCL and PEO, respectively. This was also further corroborated by performing WAXD analysis of N-S80E10L10 nanofiber blend samples after cooling from melt to different crystallization temperatures.

It was observed that for samples cooled up to 31 °C, only diffraction peaks corresponding to PEO crystals were observed. The diffraction peak corresponding to PCL crystals appeared for samples crystallized at 4 °C because of the heterogeneous nucleated PCL crystallization (please see ESI†). Fig. 6 shows the variation of different peak crystallization temperatures, as revealed from Fig. 4(c), corresponding to the PEO weight fraction in the ternary blend nanofibers. As could be observed, the T_c corresponding to the homogenous nucleation mechanism in PEO and PCL remains almost the same at different compositions. The T_c corresponding to the heterogeneous nucleation mechanism, however, was lower both for PEO and PCL when their weight fraction in the blend was less than 0.2.

However, the most interesting observation was the enhancement of the heterogeneous nucleated crystallization of PEO as well as of PCL in the PS/PEO/PCL ternary blend nanofibers compared to that in PS/PEO and PS/PCL binary blend nanofibers at nearly equivalent compositions. In the following, we discuss this observation in more detail. Fig. 4(c) shows that the crystallization exotherm between 25 and 35 °C in the N-S80E15L05 and N-S80E10L10 blend nanofibers was much more prominent compared to that between −25 and −20 °C. Hence, the heterogeneous nucleated crystallization of PEO was more dominant than the homogenous nucleated crystallization. This was observed even when the total weight fraction of PEO in the blend was less than 0.2. As already shown, in the N-S80E20L00 blend nanofibers, where the PEO weight fraction was equal to 0.2, heterogeneous nucleation was considerably suppressed and the crystallization was dominated by homogenous nucleation because the number of smaller PEO domains was significantly higher than the heterogeneities present.[62]

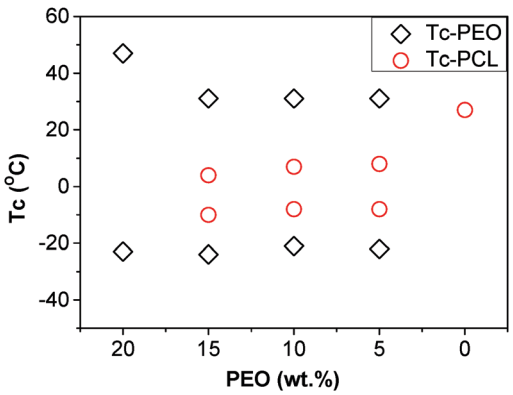

Fig. 6 Variation of crystallization peak temperatures, attributed to homogenous and heterogenous nucleation mechanisms, of PEO and PCL with respect to the PEO composition in PS/PEO/PCL blend nanofibers.

Hence, it was expected that a further reduction in the PEO weight fraction would lead to even more suppression of the heterogeneous nucleation because of further reduction in the domain volume. However, it is evident that the incorporation of PCL in the blend in some way promoted the heterogeneous nucleation mechanism in the PS/PEO/PCL ternary blend nanofibers. Similar observation was also made for the PCL crystallization. The heterogeneous nucleated crystallization of PCL observed in the exotherm between 0 and 10 °C, in PS/PEO/PCL ternary blend nanofibers, was more noticeable compared to that due to homogenous nucleated crystallization observed between −10 and 0 °C. This evidently was due to favored heterogeneous nucleation for PCL in the presence of PEO in the blend. The increase in the heterogeneous nucleation of PEO and PCL in the ternary blend could be understood using the recent concept of fluctuation-assisted crystallization proposed theoretically by Muthukumar and coworkers[76] and experimentally demonstrated by Han and coworkers.[77–79] According to this concept, the coupling between liquid–liquid phase separation (LLPS) and crystallization in polymer blends can facilitate the heterogeneous nucleated crystallization. It was observed that in polymer blends undergoing LLPS *via* spinodal decomposition, the crystallization kinetics of the crystallizable polymer was drastically affected indicating a strong coupling between the concentration fluctuation of LLPS and the nucleation of crystallization. It was proposed that the growth of concentration fluctuations induces the motion of polymer chains through inter-diffusion and a possible alignment and/or orientation of chain segments, which could assist in the formation of nuclei for crystallization.

It is plausible that in PS/PEO/PCL blend nanofibers, the PEO and PCL were partially miscible. As already discussed, PEO/PCL blends have been reported to be miscible well above the melt temperature ($T > 130$ °C) and show liquid–liquid phase separation below the UCST.[72–74] The spinodal decomposition temperature was found to be composition dependent and is about 110 °C for PEO/PCL:50/50 composition. However, since the molecular weight of PEO and PCL used in this work is much higher, the UCST for the present PEO/PCL system was expected to be much higher. Hence, UCST driven miscibility of PEO and PCL may not be the case in the present system. The limited miscibility of the PEO/PCL mixture dispersed in the PS matrix in the ternary blend electrospun nanofibers, however, could be a kinetically trapped structure due to the fast solvent evaporation during the electrospinning process and the confinement imposed by the PS matrix affecting the chain mobility. Hence, during non-isothermal crystallization, when the ternary blend nanofibers were heated up to 90 °C and subsequently cooled, the thermodynamic instability in the miscible PEO/PCL phase

 This journal is © The Royal Society of Chemistry 2017

Published on 19 January 2017. Downloaded by Synchrotron Radiation Library on 20/07/2017 02:15:51.

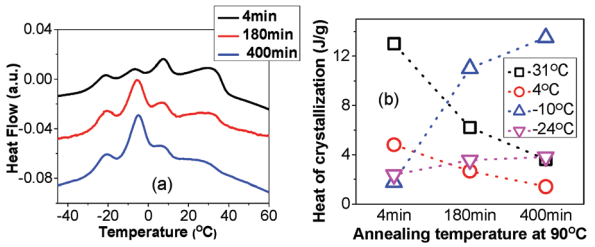

Fig. 7 DSC cooling curves of (a) N-S80E10L10 blends after melt annealing at 90 °C for different times; (b) variation of heat of crystallization corresponding to each crystallization peak with melt annealing time.

induced LLPS within the PEO/PCL domains. The LLPS occurred *via* spinodal decomposition which led to concentration fluctuations in the PEO/PCL domain and its further growth occurred such that PEO and PCL rich domains form and grow towards its liquid–liquid co-existent compositions. During this process, PEO chains diffused towards PEO-rich phases and PCL chains towards PCL-rich phases. The diffusing PEO (or PCL) chains could lead to segmental alignment and orientation during the repetitive interdiffusion. Subsequently, the diffusion induced aligned segments may attach themselves to the interface and act as the precursor for crystallization.[77–79] In order to further validate this hypothesis, the N-S80E10L10 blend nanofibers were annealed at 90 °C for 180 and 400 minutes within the DSC cell in order to allow more time for the LLPS before cooling for further crystallization. Fig. 7(a) shows the DSC cooling curves of N-S80E10L10 blend nanofibers obtained after treating the sample isothermally at 90 °C for 4, 180, and 400 minutes. It could be clearly observed that when the sample was cooled after annealing for a long time, the heterogeneous nucleated crystallization of PEO as well as that of PCL was suppressed as compared to that observed for the short isothermal treatment. This could also be observed in Fig. 7(b) which shows the variation of heat of crystallization corresponding to each crystallization peak observed in the DSC curve, with respect to the melt annealing time. The suppression of the heterogeneous nucleated crystallization peak was due to the fact that long term annealing at 90 °C allowed LLPS to move closer toward completion such that the fluctuation peaks almost saturate at the co-existent compositions. Hence, subsequent cooling led to the crystallization of PEO and PCL within their closer to pure phases and the effect of fluctuation-induced crystallization was substantially reduced.

It must be mentioned that experiments were also carried out at further lower weight fractions of the PEO/PCL mixture in the ternary blend nanofibers to observe if the fluctuation induced crystallization could still be observed. Fig. 8 shows the DSC cooling curves of the PS/PEO/PCL ternary blends where the total PEO/PCL weight fraction was 0.1. The cooling curves were obtained after annealing at 90 °C for 4 minutes. The figure shows that despite the very low weight fraction of PEO and PCL (w_{PEO} = w_{PCL} = 0.05) in the ternary blend, heterogeneous nucleation could still be observed for the respective homopolymers. In comparison, the heterogeneous nucleated crystallization was

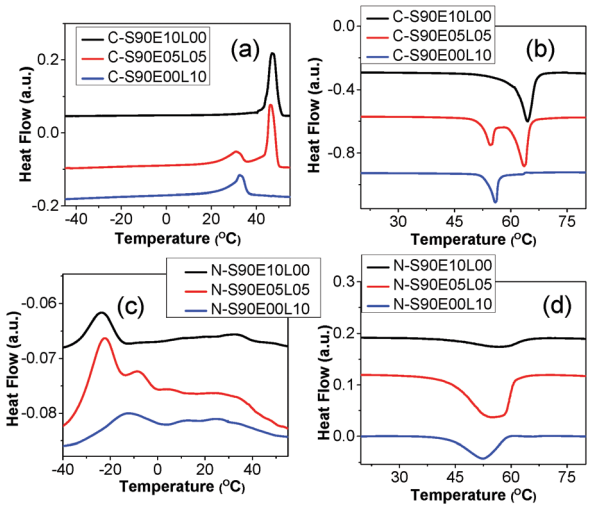

Fig. 8 DSC cooling (a and c) and heating (b and d) curves of PS/PEO/PCL blends after first heating up to 90 °C: (a and b) cast film samples and (c and d) nanofiber samples.

hardly observed in the binary PS/PEO and PS/PCL blend nanofibers even when the weight fraction of PEO and PCL was comparatively higher (w_{PEO} = w_{PCL} = 0.1). Hence, fluctuation assisted crystallization was clearly observed for the ternary blend nanofibers at a lower weight fraction of PEO/PCL blends. It must be mentioned that concentration-fluctuation and interface assisted crystallization in the PEO/PCL binary blends have also been reported earlier.[80]

However, it was shown that although PCL experienced enhanced crystallization in the presence of PEO, the effect of PCL on PEO crystallization was negligible. It must be noted that, in the present study, a similar effect of fluctuation assisted crystallization was not visible in the bulk PEO/PCL binary and PS/PEO/PCL ternary blends plausibly due to the much higher molecular weight of PEO and PCL used in this work. This further reinforces our earlier given hypothesis that fluctuation assisted crystallization in the ternary blend nanofibers was due to the limited miscibility of PEO/PCL driven by a combination of fast solvent evaporation during the electrospinning process and the confinement effect leading to the localization of PEO/PCL mixtures in smaller domains confined by the PS glassy matrix. Furthermore, the high orientation of the PEO and PCL chains due to the electrospinning process in the nanofiber may be an additional factor influencing LLPS driven crystallization.

The melting behavior of the PS/PEO/PCL blend nanofibers was similar to that of the corresponding as-casted bulk samples. The observation of two melting points corresponding to PEO and PCL homopolymers reveal that the PEO/PCL mixture displayed phase segregated crystallization behavior within the glassy PS confinement (Fig. 4(d)). The peak melting temperatures (T_m) of PEO and PCL, however, were lower than that observed in the bulk samples. This obviously was due to the restricted growth of the crystals in the confined geometry as discussed earlier in this work for PS/PCL nanofibers and PS/PEO nanofibers. However, interestingly, the T_m of PEO in the ternary blend nanofibers was found to be slightly higher

Published on 19 January 2017. Downloaded by Synchrotron Radiation Library on 20/07/2017 02:15:51.

than that in the PS/PEO binary blend nanofibers at equivalent compositions. For example, the T_m of PEO in N-S80E10L10 was 61 °C, whereas that of the PS/PEO:90/10 blend nanofiber, which has a similar weight fraction of PEO, it was found to be located at 58.5 °C. It must be noted that the T_m was still considerably less than that of bulk PEO which depicts the T_m at 67 °C. Furthermore, a similar increase in T_m was not evident for the PCL in the ternary blend nanofibers. The reason for the enhanced melting point of PEO in the ternary blend, as of now, is not clear to us. However, the enhanced heterogeneous nucleated crystallization along with the morphological evolution within the PEO/PCL domains, in the ternary blend nanofibers, plausibly could be the factors influencing the increased melting point.

The phase segregated crystallization behavior of the PEO/PCL mixture in the ternary blend nanofibers was also evidenced from the WAXS results displayed in Fig. 9. Since the total weight fraction of crystallisable components was less than 0.2, the scattering was dominated by the glassy PS phase. The N-S80E20L00 blend nanofibers displayed two peaks observed at 2θ angles of 19.2 and 23.4° corresponding to the (120) and (032) planes of a monoclinic unit cell of PEO. It is well known that the monoclinic unit cell in PEO consists of four helical chains, each of which is composed of seven monomeric units incorporated in two turns corresponding to a 7/2 helix.[81] Similarly, the N-S80E00L20 blend nanofibers displayed two peaks observed at 2θ angles of 21.3 and 23.6° corresponding to (110) and (200) planes of the orthorhombic unit cell of PCL.[82,83] The unit cell of PCL consists of an extended planar chain conformation of the molecule involving two monomer residues related by a two-fold screw axis in the chain direction. The positions of the diffraction peaks of the PEO and PCL crystallites were found to remain unchanged, in the ternary blend, with respect to the blend composition, showing that the PEO/PCL undergoes phase segregated crystallization, and their crystal structure was unperturbed in the nanofiber samples. Furthermore, the WAXS data also show that the PS/PEO/PCL ternary blend nanofibers have a poorly developed crystalline phase as evidenced from the broad halo with weakly intense diffraction peaks. The lower degree of crystallinity and the absence of coherently stacked lamellae in the ternary blend nanofibers were also clear from the SAXS results of nanofibers which were featureless, without displaying any discernible peaks (please see ESI†).

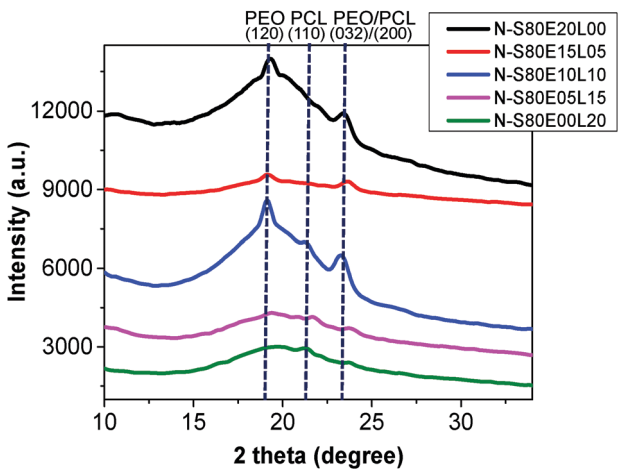

Fig. 9 WAXS profiles of PS/PEO/PCL nanofibers at room temperature.

Domain morphology of the PS/PEO/PCL blend nanofibers. The morphology of the PS/PEO/PCL blends was analyzed using SEM. For imaging the domain morphology, the PEO and PS fractions in the blends were sequentially etched using deionized water and cyclohexane, respectively. The SEM micrographs obtained after each etching step is shown in Fig. 10. It has already been shown that in the case of the PS/PEO binary blend nanofibers, when the PEO weight fraction was less than 0.2, the morphology consisted of isolated fibrils of PEO embedded in the PS matrix.[62] Similar morphology was also expected for the PS/PCL binary blends. In the case of the PS/PEO/PCL ternary blends, SEM images obtained after the first washing step with deionized water showed elongated pore-like structures on the

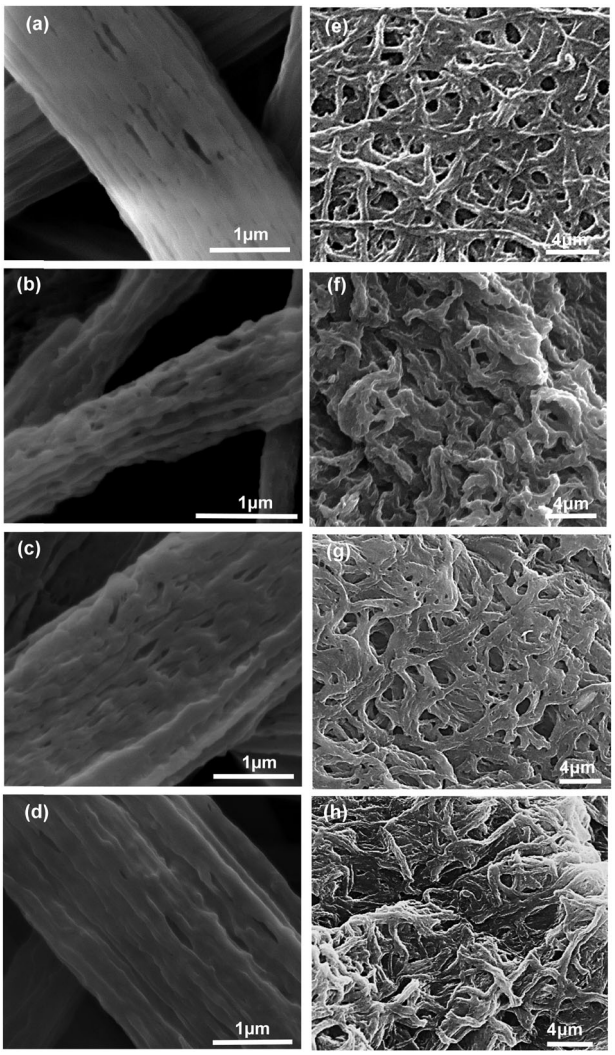

Fig. 10 SEM micrographs showing the morphology of the electrospun PS/PEO/PCL blend nanofiber samples after selective etching of the PEO phase with deionized water: (a) N-S80E20L00; (b) N-S80E15L05; (c) N-S80E10L10; (d) N-S80E05L15, and further washing with cyclohexane to remove the PS phase: (e) N-S80E00L20; (f) N-S80E15L05; (g) N-S80E10L10; (h) N-S80E05L15.

 This journal is © The Royal Society of Chemistry 2017

Published on 19 January 2017. Downloaded by Synchrotron Radiation Library on 20/07/2017 02:15:51.

surface which were formed due to the dissolution of PEO fibril domains. The pore-like structures were less visible in the N-S80E05L15 sample due to the lower concentration of PEO in the blends. Further washing of the sample with cyclohexane to etch out the PS phase led to the formation of an interconnected network of ribbon like structures. These ribbon-like structures were actually fibrils composed of PCL homopolymer since it was soluble neither in water nor in cylcohexane. The SEM images, however, did not provide unambiguous information about the coexistence of PEO and PCL phases within a domain as was observed for the cast films. However, it is reasonable to assume that the PEO/PCL phases also co-existed in the case of blend nanofibers as also evidenced from the previous discussion on DSC results.

Effect of melt annealing treatment. The crystallization behaviour discussed previously was studied by first heating the blend samples up to 90 °C which, though situated well above the T_m of PEO and PCL, was below the T_g of PS (T_g^{PS}). Hence, in this case, the crystallization of PEO/PCL domains occurred under the hard confinement imposed by the glassy PS matrix. Since the PEO/PCL domains with fibrillar geometry may be metastable in nature, it is of interest to explore if such a domain morphology would be perturbed after annealing the blends above the T_g^{PS} of PS and how such a morphological perturbation would influence the crystallization behaviour. For this study, N-S80E15L05 and N-S80E10L10 ternary blend samples were crystallized after annealing at different temperatures ($T_a > T_g^{PS}$) for 30 min. Fig. 11 shows the DSC cooling and reheating curves of N-S80E10L10 ternary blend nanofibers after the annealing treatment. The most significant observation from the cooling curves was a marked enhancement in the crystallization exotherm, in the N-S80E10L10 ternary blend samples, attributed to the homogenous nucleated crystallization of PEO, as the melt annealing temperature was increased. Moreover, the T_c corresponding to the heterogeneous crystallization of PEO shifted from 31 to 40 °C as the melt annealing temperature was increased from 90 to 160 °C. However, for PCL, the homogenous nucleated crystallization became slightly more dominant when the melt annealing temperature was increased. The observed crystallization behavior for different melt annealing temperatures could be explained as follows.

When T_a was lower than T_g^{PS}, the PEO/PCL fibrillar domain morphology formed during electrospinning was largely retained due to the hard confinement imposed by the PS glassy matrix. In this case, the crystallization behavior of PEO and PCL was governed by a combination of confinement imposed by the PS glassy matrix on the PEO/PCL fibrillar domains and fluctuation driven crystallization, as already discussed. However, at T_a situated above T_g^{PS}, the breakup of the fibrillar PEO/PCL domains driven by the Rayleigh–Plateau instability[84] occurred, leading to a reduction of domain size. Nevertheless, the reduction in domain size should have led to more dominant homogenous nucleated crystallization because of the decreased domain volume for accommodating heterogeneities. This suggested that some other factor was also influencing crystallization and had a more dominant effect. Hence, two more factors were considered. The first was that at higher T_a, apart from the domain breakup, coalescence between the neighboring PEO/PCL domains tended to take place spontaneously to reduce the interfacial energy. This coarsening process increased the size of the domains. Hence, the ultimate PEO/PCL domain size and morphology were dictated by competition between the Plateau–Rayleigh instability induced domain breakup and the coalescence of the resulting domains. The dominance of domain coalescence was expected to favor heterogeneous nucleation because of increased domain volume to accommodate the heterogeneities. The second additional factor which was considered was the miscibility of the homopolymers within the PEO/PCL domain.

As discussed previously, the PEO/PCL blends in the ternary blend nanofibers plausibly were partially miscible due to the kinetic effect imposed by the fast electrospinning process as well as due to their confinement within the limited domain volumes embedded in the glassy PS matrix. The softening of the PS matrix during high temperature annealing plausibly aided the phase separation within the PEO/PCL domain, driven further by the increased mobility of the polymer chains, resulting in more pure PEO and PCL phases. Furthermore, the energetics of the ternary system was such that, within the PEO/PCL domain, the PEO was the dispersed phase as already shown in Fig. 5 for cast films. Hence, the phase separation was likely to increase the PEO domain size within the PEO/PCL phase favoring heterogeneous nucleated crystallization. The exact scenario may be complex because of the interplay of different factors discussed and is not very clear to us at present. Furthermore, the discussion made here for enhanced heterogeneous crystallization of PEO does not explain the increased homogenous nucleated crystallization of PCL. This plausibly could be due to the increased heterogeneous nucleated crystallization of PEO such that the crystallization of PCL occurred within the confinement not only imposed by the glassy PS matrix but also by the crystalline PEO phase.

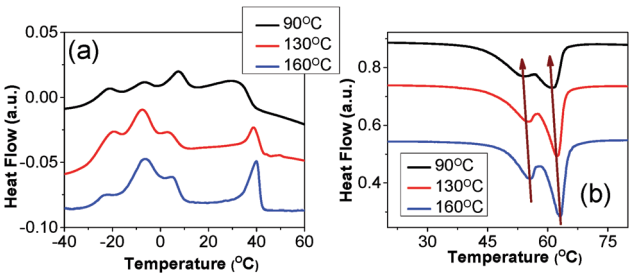

Fig. 11 DSC cooling (a) and heating (b) curves of the N-S80E10L10 sample after thermal treatment of the samples to different melt conditioning temperatures (T_a).

Experimental

Materials

Poly(ethylene oxide) (PEO) ($M_v \sim 400\,000$ g mol^{-1}), poly(ε-caprolactone) (PCL) ($M_w \sim 60\,000$ g mol^{-1}) and polystyrene (PS) ($M_w \sim 190\,000$ g mol^{-1}) were purchased from Sigma Aldrich.

Published on 19 January 2017. Downloaded by Synchrotron Radiation Library on 20/07/2017 02:15:51.

Dimethylformamide (DMF), dichloromethane (DCM) and cyclohexane were obtained from Merck Chemicals and used as they are.

Sample preparation

PS/PCL binary blend. PS and PCL were added into the solvent mixture of DMF/DCM in a 70/30 ratio for overnight swelling, after which the solution was stirred for 30 minutes at 80 °C and then at room temperature for 24 hours to obtain a homogeneous polymer solution. The weight fraction of PCL in the PS/PCL blends was varied from 0.1 to 0.3. Bulk samples were prepared by casting the blend solution on a Petri-dish followed by evaporating the solvent under ambient conditions. The blend nanofibers were prepared by electrospinning their solutions under optimized conditions. The optimum conditions used for electrospinning to obtain bead-free uniform nanofibers and sample nomenclatures for the PS/PCL blends are given in Table 1. The bulk and nanofiber blend samples were differentiated by adding the prefixes C and N, respectively, to the blend composition codes. All the samples were vacuum dried for at least 2 days before further analysis.

PS/PEO/PCL ternary blends. The ternary polymer mixture of PS, PEO and PCL blends was prepared by taking a pre-weighed physical mixture of the three components in the required ratios and dissolving it in a DMF/DCM (70/30) mixture by first keeping it for overnight swelling and then further stirring for half an hour at 80 °C. The solution was further stirred at room temperature for 24 hours to obtain a homogeneous polymer solution. The total weight fraction of the PEO/PCL mixture was varied up to 0.2 in the blend thereby keeping PS as the matrix-forming polymer. Furthermore, within the PEO/PCL mixture the weight fractions of PEO and PCL were also varied. Table 2 lists the details of the sample composition, sample codes and electrospinning parameters used.

Characterization techniques

Differential scanning calorimetry (DSC). A TA Q 2000 DSC instrument was used to study the crystallization and melting behaviour of the blends. The non-isothermal crystallization of the blend samples was carried out by heating them from 30 to 90 °C (or at the desired annealing temperature) at the heating rate of 10 °C min^{-1} and further holding for 4 min (or more) to erase the previous thermal history. Subsequently, the samples were cooled to −50 °C at the rate of 5 °C min^{-1} and reheated up to 90 °C at the rate of 10 °C min^{-1}. The isothermal crystallization studies were carried out by quenching from the melt state to the desired crystallization temperature in the DSC at 200 °C min^{-1} followed by crystallization for at least one hour. The sample was then heated to 90 °C at 10 °C min^{-1} to record the melting endotherms.

Scanning electron microscopy (SEM). The surface morphology of the samples was observed using a scanning electron microscope (SEM), ZEISS EVO 50. Before observation, the samples were sputter-coated with a thin layer of gold to avoid the accumulation of electrons on the surface of the samples. In order to develop contrast, the samples were washed either with water or cyclohexane to etch out PEO or PS, respectively.

Small angle X-ray scattering (SAXS) and wide angle X-ray scattering (WAXS) measurements. The combined SAXS/WAXS experiments were conducted at the BL23A SWAXS beamline of the National Synchrotron Radiation Research Center (NSRRC) located at Hsinchu, Taiwan. The energy of the X-ray source was 15 keV (λ = 0.083 nm). A two-dimensional Mar CCD detector (512 × 512 pixel resolution) at the sample-to-detector distance of 2259 mm was used to record the 2-D SAXS scattering pattern, and a CMOS flat panel X-ray detector (C9728DK with the area of 52.8 mm^2) at the sample to detector distance of 124.53 mm was employed to record the 2-D WAXS scattering pattern. The SAXS/WAXS measurements were performed for the isothermally crystallized samples.

Conclusions

The crystallization behavior of PEO and PCL in the cast films and electrospun nanofibers of a PS/PEO/PCL ternary blend has been investigated in detail. The crystallization behavior of the PEO/PCL mixture in the ternary blend films was similar to that observed for bulk PEO and PCL which took place through a heterogeneous nucleation mechanism. However, the PS/PEO/PCL ternary blend nanofibers depicted significantly different crystallization behavior where both PEO and PCL crystallized *via* a heterogeneous as well as a homogenous nucleation mechanism. The observation of homogenous nucleation for PEO and PCL in the ternary blend nanofibers was expected considering that the PS/PEO and PS/PCL binary blend nanofibers at equivalent weight fractions of PEO and PCL also crystallized mostly *via* homogenous nucleation. The homogenous nucleation was due to the small PEO/PCL domain size such that a large number of such domains were free form heterogeneity. However, interestingly, the heterogeneous nucleation of PEO and PCL was much more dominant in the ternary blend nanofibers, even at much lower weight fractions of PEO and PCL. This was contrary to the inference drawn from the crystallization behavior of PS/PEO and PS/PCL binary blend nanofibers. The enhanced heterogeneous nucleation activity in the ternary blend was attributed to the coupling between the crystallization and the concentration fluctuation of liquid–liquid phase separation (LLPS) of the PEO/PCL mixture dispersed in the PS matrix during non-isothermal cooling of the blend nanofibers. Furthermore, it was observed that thermal treatment of the PS/PEO/PCL blend nanofibers above the glass transition temperature of PS led to further enhancement in the heterogeneous crystallization of PEO because of a complex interplay between Plateau–Rayleigh instability-induced domain breakup and its further coalescence and demixing within the PEO/PCL domains. However, the heterogeneous nucleation of PCL was suppressed under similar thermal treatment plausibly due to extra confinement imposed by the crystallized PEO apart from that of the PS glassy matrix. The present study shows that the crystallization and dynamics of phase separation in similar blend systems could be very different to those in bulk due to

 This journal is © The Royal Society of Chemistry 2017

Published on 19 January 2017. Downloaded by Synchrotron Radiation Library on 20/07/2017 02:15:51.

the confinement effect as well as the orientated structures in the electrospun nanofibers.

Acknowledgements

This work was supported by the Council for Scientific and Industrial Research (CSIR) under grant no. 22(0707)/15/EMR-II.

Notes and references

1 M. Berggren, O. Inganäs, G. Gustafsson, J. Rasmusson, M. R. Andersson, T. Hjertberg and O. Wennerström, *Nature*, 1994, **372**, 444–446.
2 N. Ploypetchara, P. Suppakul, D. Atong and C. Pechyen, *Energy Procedia*, 2014, **56**, 201–210.
3 D. R. Paul and L. M. Robeson, *Polymer*, 2008, **49**, 3187–3204.
4 Y. Okabe, H. Murakami, N. Osaka, H. Saito and T. Inoue, *Polymer*, 2010, **51**, 1494–1500.
5 Y. Kong and J. N. Hay, *Polymer*, 2002, **43**, 1805–1811.
6 Q. Guo, C. Harrats, G. Groeninckx, H. Reynaers and M. H. J. Koch, *Polymer*, 2001, **42**, 6031–6041.
7 Q. Guo, C. Harrats, G. Groeninckx and M. H. J. Koch, *Polymer*, 2001, **42**, 4127–4140.
8 R. K. Krishnaswamy and D. S. Kalika, *Polym. Eng. Sci.*, 1996, **36**, 786–796.
9 V. Ferreiro, J. F. Douglas, J. A. Warren and A. Karim, *Phys. Rev. E: Stat., Nonlinear, Soft Matter Phys.*, 2002, **65**, 042802.
10 M. Avella, E. Martuscelli and M. Raimo, *Polymer*, 1993, **34**, 3234–3240.
11 M. Avella, E. Martuscelli, G. Orsello, M. Raimo and B. Pascucci, *Polymer*, 1997, **38**, 6135–6143.
12 Z. Qiu, T. Ikehara and T. Nishi, *Polymer*, 2003, **44**, 2503–2508.
13 E. Blümm and A. J. Owen, *Polymer*, 1995, **36**, 4077–4081.
14 N. Koyama and Y. Doi, *Polymer*, 1997, **38**, 1589–1593.
15 Y. Hu, H. Sato, J. Zhang, I. Noda and Y. Ozaki, *Polymer*, 2008, **49**, 4204–4210.
16 H.-J. Chiu, H.-L. Chen and J.-S. Lin, *Polymer*, 2001, **42**, 5749–5754.
17 T. Ikehara, Y. Nishikawa and T. Nishi, *Polymer*, 2003, **44**, 6657–6661.
18 T. Ikehara, H. Kimura and Z. Qiu, *Macromolecules*, 2005, **38**, 5104–5108.
19 Z. Qiu, T. Ikehara and T. Nishi, *Macromolecules*, 2002, **35**, 8251–8254.
20 Y.-L. Loo, R. A. Register, A. J. Ryan and G. T. Dee, *Macromolecules*, 2001, **34**, 8968–8977.
21 M.-S. Hsiao, J. X. Zheng, S. Leng, R. M. Van Horn, R. P. Quirk, E. L. Thomas, H.-L. Chen, B. S. Hsiao, L. Rong, B. Lotz and S. Z. D. Cheng, *Macromolecules*, 2008, **41**, 8114–8123.
22 H. Wang, J. K. Keum, A. Hiltner and E. Baer, *Macromolecules*, 2009, **42**, 7055–7066.
23 C.-L. Liu, M.-C. Lin, H.-L. Chen and A. J. Műller, *Macromolecules*, 2015, **48**, 4451–4460.
24 M. V. Massa and K. Dalnoki-Veress, *Phys. Rev. Lett.*, 2004, **92**, 255509.
25 T.-M. Chung, T.-C. Wang, R.-M. Ho, Y.-S. Sun and B.-T. Ko, *Macromolecules*, 2010, **43**, 6237–6240.
26 M. Pan, L. Yang, J. Wang, S. Tang, G. Zhong, R. Su, M. K. Sen, M. K. Endoh, T. Koga and L. Zhu, *Macromolecules*, 2014, **47**, 2632–2644.
27 A. Taden and K. Landfester, *Macromolecules*, 2003, **36**, 4037–4041.
28 M.-C. Lin, B. Nandan and H.-L. Chen, *Soft Matter*, 2012, **8**, 7306.
29 R. M. Michell and A. J. Müller, *Prog. Polym. Sci.*, 2016, **54–55**, 183–213.
30 R. M. Michell, I. Blaszczyk-Lezak, C. Mijangos and A. J. Müller, *J. Polym. Sci., Part B: Polym. Phys.*, 2014, **52**, 1179–1194.
31 A. Samanta, B. Nandan and R. K. Srivastava, *J. Colloid Interface Sci.*, 2016, **471**, 29–36.
32 S. Nakagawa, H. Marubayashi and S. Nojima, *Eur. Polym. J.*, 2015, **70**, 262–275.
33 L. Sun, L. Zhu, Q. Ge, R. P. Quirk, C. Xue, S. Z. Cheng, B. S. Hsiao, C. A. Avila-Orta, I. Sics and M. E. Cantino, *Polymer*, 2004, **45**, 2931–2939.
34 R.-M. Ho, F.-H. Lin, C.-C. Tsai, C.-C. Lin, B.-T. Ko, B. S. Hsiao and I. Sics, *Macromolecules*, 2004, **37**, 5985–5994.
35 L. Zhu, B. H. Calhoun, Q. Ge, R. P. Quirk, S. Z. D. Cheng, E. L. Thomas, B. S. Hsiao, F. Yeh, L. Liu and B. Lotz, *Macromolecules*, 2001, **34**, 1244–1251.
36 P. Huang, Y. Guo, R. P. Quirk, J. Ruan, B. Lotz, E. L. Thomas, B. S. Hsiao, C. A. Avila-Orta, I. Sics and S. Z. D. Cheng, *Polymer*, 2006, **47**, 5457–5466.
37 Y. Suzuki, M. Steinhart, M. Kappl, H.-J. Butt and G. Floudas, *Polymer*, 2016, **99**, 273–280.
38 Y. Suzuki, M. Steinhart, R. Graf, H.-J. Butt and G. Floudas, *J. Phys. Chem. B*, 2015, **119**, 14814–14820.
39 Y. Suzuki, M. Steinhart, H.-J. Butt and G. Floudas, *J. Phys. Chem. B*, 2015, **119**, 11960–11966.
40 Y. Suzuki, H. Duran, M. Steinhart, M. Kappl, H.-J. Butt and G. Floudas, *Nano Lett.*, 2015, **15**, 1987–1992.
41 X. Dai, J. Niu, Z. Ren, X. Sun and S. Yan, *J. Phys. Chem. B*, 2016, **120**, 843–850.
42 B. Sanz, I. Blaszczyk-Lezak, C. Mijangos, J. K. Palacios and A. J. Müller, *Langmuir*, 2016, **32**, 7860–7865.
43 Y. Yao, T. Sakai, M. Steinhart, H.-J. Butt and G. Floudas, *Macromolecules*, 2016, **49**, 5945–5954.
44 R. Kato, S. Nakagawa, H. Marubayashi and S. Nojima, *Macromolecules*, 2016, **49**, 5955–5962.
45 Y. Suzuki, H. Duran, M. Steinhart, H.-J. Butt and G. Floudas, *Soft Matter*, 2013, **9**, 2621.
46 Y. Suzuki, H. Duran, W. Akram, M. Steinhart, G. Floudas and H.-J. Butt, *Soft Matter*, 2013, **9**, 9189.
47 H. Duran, M. Steinhart, H.-J. Butt and G. Floudas, *Nano Lett.*, 2011, **11**, 1671–1675.
48 P. Huang, L. Zhu, Y. Guo, Q. Ge, A. J. Jing, W. Y. Chen, R. P. Quirk, S. Z. D. Cheng, E. L. Thomas, B. Lotz, B. S. Hsiao, C. A. Avila-Orta and I. Sics, *Macromolecules*, 2004, **37**, 3689–3698.

Published on 19 January 2017. Downloaded by Synchrotron Radiation Library on 20/07/2017 02:15:51.

49 S. Nakagawa, K. Kadena, T. Ishizone, S. Nojima, T. Shimizu, K. Yamaguchi and S. Nakahama, *Macromolecules*, 2012, **45**, 1892–1900.
50 J. Martín, A. Nogales and C. Mijangos, *Macromolecules*, 2013, **46**, 7415–7422.
51 Y. Guan, G. Liu, G. Ding, T. Yang, A. J. Müller and D. Wang, *Macromolecules*, 2015, **48**, 2526–2533.
52 C. Bishop and D. Teeters, *Electrochim. Acta*, 2009, **54**, 4084–4088.
53 A. Houachtia, P. Alcouffe, G. Boiteux, G. Seytre, J.-F. Gérard and A. Serghei, *Nano Lett.*, 2015, **15**, 4311–4316.
54 C.-Y. Chu, H.-L. Chen, M.-S. Hsiao, J.-H. Chen and B. Nandan, *Macromolecules*, 2010, **43**, 3376–3382.
55 Y.-Y. Huang, B. Nandan, H.-L. Chen, C.-S. Liao and U.-S. Jeng, *Macromolecules*, 2004, **37**, 8175–8179.
56 S. Balijepalli, J. M. Schultz and J. S. Lin, *Macromolecules*, 1996, **29**, 6601–6611.
57 S. Z. D. Cheng and B. Wunderlich, *J. Polym. Sci., Part B: Polym. Phys.*, 1986, **24**, 577–594.
58 S. Z. D. Cheng and B. Wunderlich, *J. Polym. Sci., Part B: Polym. Phys.*, 1986, **24**, 595–617.
59 S. Z. D. Cheng, H. S. Bu and B. Wunderlich, *J. Polym. Sci., Part B: Polym. Phys.*, 1988, **26**, 1947–1964.
60 M. L. Arnal, F. López-Carrasquero, E. Laredo and A. J. Müller, *Eur. Polym. J.*, 2004, **40**, 1461–1476.
61 Y. Suzuki, H. Duran, M. Steinhart, H.-J. Butt and G. Floudas, *Macromolecules*, 2014, **47**, 1793–1800.
62 P. Samanta, T. Velmayil, S. Singh, R. Srivastava, B. Nandan, C.-L. Liu and H.-L. Chen, *Soft Matter*, 2016, **12**, 5110–5120.
63 M. Pakravan, M.-C. Heuzey and A. Ajji, *Polymer*, 2011, **52**, 4813–4824.
64 Z.-M. Huang, Y.-Z. Zhang, M. Kotaki and S. Ramakrishna, *Compos. Sci. Technol.*, 2003, **63**, 2223–2253.
65 S. L. Shenoy, W. D. Bates and G. Wnek, *Polymer*, 2005, **46**, 8990–9004.
66 M. G. McKee, G. L. Wilkes, R. H. Colby and T. E. Long, *Macromolecules*, 2004, **37**, 1760–1767.
67 L. I. Silva, Ú. M. Montoya Rojo and C. C. Riccardi, *Polym. Eng. Sci.*, 2016, DOI: 10.1002/pen.24480.
68 H.-L. Chen, J.-C. Wu, T.-L. Lin and J. S. Lin, *Macromolecules*, 2001, **34**, 6936–6944.
69 H.-L. Chen, S.-C. Hsiao, T.-L. Lin, K. Yamauchi, H. Hasegawa and T. Hashimoto, *Macromolecules*, 2001, **34**, 671–674.
70 H.-L. Chen, S.-Y. Lin, Y.-Y. Huang, F.-C. Chiu, W. Liou and J. S. Lin, *Macromolecules*, 2002, **35**, 9434–9440.
71 K. Shin, E. Woo, Y. G. Jeong, C. Kim, J. Huh and K.-W. Kim, *Macromolecules*, 2007, **40**, 6617–6623.
72 W.-T. Chuang, K.-S. Shih and P.-D. Hong, *J. Polym. Res.*, 2005, **12**, 197–204.
73 W.-T. Chuang, U.-S. Jeng, H.-S. Sheu and P.-D. Hong, *Macromol. Res.*, 2006, **14**, 45–51.
74 J. Li, Y. Zhang, Y. Jiacuo, Y. Shang, H. Huo and S. Jiang, *Polym. Bull.*, 2012, **68**, 1405–1423.
75 *Polymer Handbook*, ed. J. Brandrup, E. H. Immergut and E. A. Grulke, Wiley, New York, Chichester, 4th edn, 2004.
76 M. K. Mitra and M. Muthukumar, *J. Chem. Phys.*, 2010, **132**, 184908.
77 W. Shi, F. Chen, Y. Zhang and C. C. Han, *ACS Macro Lett.*, 2012, **1**, 1086–1089.
78 X. Zhang, Z. Wang, X. Dong, D. Wang and C. C. Han, *J. Chem. Phys.*, 2006, **125**, 24907.
79 X. Zhang, Z. Wang, M. Muthukumar and C. C. Han, *Macromol. Rapid Commun.*, 2005, **26**, 1285–1288.
80 H. Huo, C. Guo, J. Zhou and X. Zhao, *Colloid Polym. Sci.*, 2014, **292**, 971–983.
81 Y. Takahashi, I. Sumita and H. Tadokoro, *J. Polym. Sci., Part B: Polym. Phys.*, 1973, **11**, 2113–2122.
82 G. Floudas, G. Reiter, O. Lambert and P. Dumas, *Macromolecules*, 1998, **31**, 7279–7290.
83 H. Hu and D. L. Dorset, *Macromolecules*, 1990, **23**, 4604–4607.
84 J. D. McGraw, J. Li, D. L. Tran, A.-C. Shi and K. Dalnoki-Veress, *Soft Matter*, 2010, **6**, 1258.

 This journal is © The Royal Society of Chemistry 2017